

Article

# Crystallization Behavior of Ceritinib: Characterization and Optimization Strategies

Iva Zokić  and Jasna Prlić Kardum \* 

Department of Mechanical and Thermal Process Engineering, Faculty of Chemical Engineering and Technology, University of Zagreb, Marulićev trg 19, 10000 Zagreb, Croatia; izokic@fkit.unizg.hr

\* Correspondence: jprlic@fkit.unizg.hr

**Abstract:** Because of the specific thermodynamic properties of active pharmaceutical ingredients, the process of crystallization often meets implementation challenges in the pharmaceutical industry. Therefore, it is essential to select the appropriate method and system for the crystallization of a drug. Ceritinib, an active ingredient in the treatment of lung cancer, was formed as a result of pH modification during the cooling crystallization of ceritinib dihydrochloride solution. By carrying out processes in various solvent systems, several polymorphs were produced. A combination of forms B and C was generated in the ethanol–water system, resulting in smaller crystals. The acetone–water system produced pure form A, which has larger crystals and is more applicable for forthcoming studies. To additionally enhance granulometric properties, ceritinib form A was recrystallized in tetrahydrofuran at different temperatures using antisolvent crystallization. Crystallization at a higher saturation temperature results in larger and more compact crystals, which enhances filtration and drying.

**Keywords:** active pharmaceutical ingredient; batch crystallization; ceritinib; drying; solubility



**Citation:** Zokić, I.; Prlić Kardum, J. Crystallization Behavior of Ceritinib: Characterization and Optimization Strategies. *ChemEngineering* **2023**, *7*, 84. <https://doi.org/10.3390/chemengineering7050084>

Academic Editor: Alirio E. Rodrigues

Received: 25 August 2023

Revised: 9 September 2023

Accepted: 12 September 2023

Published: 14 September 2023



**Copyright:** © 2023 by the authors. Licensee MDPI, Basel, Switzerland. This article is an open access article distributed under the terms and conditions of the Creative Commons Attribution (CC BY) license (<https://creativecommons.org/licenses/by/4.0/>).

## 1. Introduction

Crystallization is a separation process utilized in the chemical, food, and pharmaceutical industries to purify or produce a new solid phase from a solution, suspension, or melt [1]. Various factors, such as temperature, agitation, saturation, supersaturation, or the presence of additives, can influence the implementation and outcome of the crystallization process by impacting the crystal growth, morphology, and internal structure of obtained crystals [2]. Crystalline form, size, and shape directly affect the physical and chemical properties of solids such as solubility and dissolution rate, as well as downstream processes such as filtration, milling, drying, or tableting; therefore, it is important to have control over the crystallization process.

In the pharmaceutical industry, crystallization is beneficial for the separation of intermediates and the production and purification of active pharmaceutical ingredients (APIs) [1,3]. Production of APIs requires obtaining a product of high purity and good physical properties, which is why great attention is paid to the selection of the solvent system in which the crystallization is carried out. The solvent system used for the crystallization of an organic compound can influence the efficiency of the process, resulting morphology, flowability, and compressibility of obtained crystals, and also application possibilities. A poor solvent selection can cause a slew of issues during crystallization and, as a result, difficulties with crystal handling during downstream processes [4,5]. The granulometric characteristics of the resultant crystals can be altered by adjusting the process parameters, but the crystal structure of big organic molecules, such as APIs, is determined by the interactions of the molecules in the system [6]. Due to differences in the crystal structure, polymorphs can have distinct mechanical and physicochemical characteristics, such as solubility, bioavailability, stability, melting point, or color [7]. Consequently, solvent

screening is commonly reported when searching for various polymorphs. In addition, the discovery of a novel polymorph allows for the application of a new patent and the release of a novel drug, which usually generates a great profit. When the crystallization process is optimized, it is possible not only to increase profit but also to address the issue of APIs with poor solubility. Approximately 40% of drugs available today belong to Class II or Class IV under the Biopharmaceutics Classification System (BCS), characterized by low solubility and high permeability or low solubility and low permeability through the intestinal membrane, respectively.

Ceritinib (CRT) is a pharmaceutical compound classified under the BCS as Class IV. It functions as an inhibitor of anaplastic lymphoma kinase (ALK) and is primarily employed in the treatment of metastatic non-small-cell lung cancer that is positive for ALK [8]. The IUPAC name of CRT ( $C_{28}H_{36}ClN_5O_3S$ ) is 5-chloro-2-N-(5-methyl-4-piperidin-4-yl-2-propan-2-yloxyphenyl)-4-N-(2-propan-2-ylsulfonylphenyl)pyrimidine-2,4-diamine, and its molar mass is 558.1 g/mol. There are three known polymorphs of CRT, A, B, and C, whose production is usually dependent on the solvent system employed during their synthesis [9]. Problems in the pharmaceutical industry are frequently related to difficulties in finding an appropriate solvent system and process parameters for crystallization implementation, which directly influence the granulometric characteristics of produced crystals. Previous studies on CRT have examined the effect of pH value on the solubility, crystallographic details of various crystal structures, and medical applications of CRT, including maximum tolerated dose, safety, and pharmacokinetics, as well as its antitumor activity [8,10]. In this study, the solubility of CRT in various solvents was determined within a defined temperature range. The aim was to identify the required parameters for optimizing the crystallization process and obtaining CRT crystals with improved granulometric characteristics, thereby facilitating subsequent filtration and drying processes.

## 2. Materials and Methods

CRT dihydrochloride was obtained from Hui Chem Co. Ltd. (Shanghai, China). Acetone, ethanol, isopropanol, methanol, sodium hydroxide, and tetrahydrofuran (THF) were obtained from Lachner (Neratovice, Czech Republic). All chemicals were used with AR purity. For the recrystallization of CRT, deionized water was used as an antisolvent. All crystallization experiments were conducted using *CrystalSCAN* (E2153, h.e.l Ltd., Borehamwood, UK) batch reactors with turbidity probes and disc turbine impellers with 6 blades inclined at a 45° angle (RT6-45).

### 2.1. Preparation of CRT from CRT Dihydrochloride

Since CRT is the API in the commercial drug, it was necessary to convert from CRT dihydrochloride to CRT. When choosing the solvent systems for the production of CRT from CRT dihydrochloride, the solubility of CRT dihydrochloride in water and a number of organic solvents was taken into account. At 25 °C, the solubility of CRT dihydrochloride was determined in pure solvents and in solvent mixtures with various water contents. CRT dihydrochloride was added in excess until the turbidity was constant, indicating that the salt stopped dissolving. Afterward, the solution was filtered through a CHROMAFIL® Xtra PET-45/25 filter (MACHEREY-NAGEL, Düren, Germany), and the mass of dissolved CRT dihydrochloride was determined gravimetrically using a moisture analyzer (*MLS 50-3C*, Kern&Sohn, Balingen, Germany).

Solvent mixtures with the most promising results (AC–W 3:1 and EtOH–W 3:1) were chosen for further work. In order to examine the influence of the initial saturation temperature on the granulometric properties, crystallization was conducted in the aforementioned systems with starting temperatures of 35 and 45 °C. To prepare CRT from CRT dihydrochloride, the salt was added to the AC–W 3:1 and EtOH–W 3:1 systems in amounts sufficient to achieve saturation. The crystallizer was heated to a temperature 5 °C above saturation to ensure that all particles had dissolved, thus avoiding spontaneous nucleation. After dissolving the salt, the solution pH was adjusted with 10 wt.% sodium hydroxide solution

until there was a visible change in color from yellow to white ( $\text{pH} \approx 11$ ) which indicates the transition from salt to API form. The crystallization process was carried out at a constant cooling rate ( $15\text{ }^\circ\text{C/h}$ ), and the resulting crystals were filtered and dried in a vacuum dryer. Afterward, the crystals were weighed and then characterized. The crystallization efficiency for all experiments was calculated by dividing the mass of the obtained crystals by the mass of dissolved CRT dihydrochloride.

## 2.2. Recrystallization of CRT Form A

To further purify crystals of CRT form A obtained from the AC–W 3:1 solvent system, solubility studies were conducted to determine a solvent and antisolvent suitable for recrystallization. According to the obtained solubility data, THF was chosen for further investigation. The solubility of CRT form A was determined in THF in the temperature range of  $5\text{--}55\text{ }^\circ\text{C}$  with a step of  $5\text{ }^\circ\text{C}$ . The experimental mole fraction solubility of CRT in said solvent was calculated from obtained masses using the equation:

$$x_{\text{exp}} = \frac{m_{\text{CRT}}/M_{\text{CRT}}}{m_{\text{CRT}}/M_{\text{CRT}} + m_{\text{THF}}/M_{\text{THF}}} \quad (1)$$

where  $M_{\text{CRT}}$  and  $M_{\text{THF}}$  represent the molar masses of CRT and THF, while  $m_{\text{CRT}}$  and  $m_{\text{THF}}$  are masses of CRT and THF, respectively.

Saturated solutions of CRT in THF at  $35$  or  $45\text{ }^\circ\text{C}$  were added to the batch reactor. The reactor was heated at a constant temperature with a mixing rate of  $300\text{ rpm}$ . Deionized water was used as an antisolvent and added at a constant volume rate ( $3\text{ mL/min}$ ) using a syringe pump. Aliquots of  $1\text{ mL}$  were withdrawn at predetermined time intervals, filtered with a CHROMAFIL<sup>®</sup> Xtra PET-45/25 filter and dried using a moisture analyzer to determine the residual concentration of CRT. The experiment was finished when the concentration was  $0\text{ g}_{\text{CRT}}/\text{g}_{\text{solvent}}$ . Additionally, the influence of the initial saturation temperature on the morphology and drying kinetics of CRT form A crystals was observed.

## 2.3. Filtration and Drying

The crystals obtained by recrystallization from THF with the addition of water as an antisolvent were subjected to filtration and drying in order to assess the influence of the initial saturation temperature on the crystal morphology and, consequently, on the aforementioned unit operations. Approximately equal masses of crystals obtained at different saturation temperatures were vacuum filtered using a Buchner funnel and washed with cold deionized water under the same conditions. The filter cakes were dried at  $60\text{ }^\circ\text{C}$  using a moisture analyzer to a constant mass. The data were collected automatically every  $30\text{ s}$ . From the experimentally obtained dependence of CRT moisture content on time, critical moisture content and velocity of drying were calculated.

## 2.4. Characterization of Crystals

Internal structures of all obtained crystals were characterized by X-ray powder diffraction (XRD 6000, Shimadzu, Kyoto, Japan). X-ray powder diffraction with a Cu-K radiation source of wavelength  $\lambda = 1.54059\text{ \AA}$  was used to identify pure CRT forms. A  $40\text{ kV}$  voltage and a current of  $30\text{ mA}$  were applied, with data gathered between  $2\theta = 5\text{--}40^\circ$  using a  $0.02^\circ$  step and a  $0.6\text{ s}$  hold each step. The shape and size of the crystals were determined by light microscopy (BA 200, Motic, Wetzlar, Germany) and the particle size distribution (PSD) was determined using laser diffraction (SALD-3101, Shimadzu).

# 3. Results and Discussion

## 3.1. Preparation of CRT from CRT Dihydrochloride

The solubility of CRT dihydrochloride was determined at room temperature ( $25\text{ }^\circ\text{C}$ ) in acetone, ethanol, isopropanol, methanol, and water. As shown in Table 1, the solubility of CRT dihydrochloride is the highest in water and the lowest in acetone, ethanol, and isopropanol. Considering the literature values [11] that determine a drug's solubility in

a certain medium, it was concluded that CRT dihydrochloride is freely soluble in water, sparingly soluble in ethanol, and slightly soluble in acetone and isopropanol.

**Table 1.** Solubility of CRT dihydrochloride in water and different organic solvents at 25 °C.

Solvent	$c_{\text{sat}} \text{ gCRT/g}_{\text{solvent}}$
W	0.278
MetOH	0.229
EtOH	0.039
AC	0.007
IP	0.003

AC—acetone, EtOH—ethanol, IP—isoopropanol, MetOH—methanol, W—water.

Since CRT dihydrochloride has very high solubility in water, which is generally the best solvent for crystallization, the process was carried out in mixtures of water and solvents that exhibited slight solubility of CRT dihydrochloride. The preparation of pure forms of CRT was, therefore, conducted in solvent systems containing different volume ratios of water and acetone, ethanol, or isopropanol, which are shown in Table 2. After conducting the solubility studies, a 10 wt.% solution of sodium hydroxide was added to adjust the pH using a syringe pump. The pH value was adjusted until a visible color change from pale yellow to orange and then white was observed and the pH value was between 10.8 and 11.9 in all solvent systems. Because the dihydrochloride solutions were extremely acidic with pH values ranging from 0.8 to 1.8, the addition of sodium alkali resulted in neutralization of the solutions, indicated by the visible change in color. Adjustment of solution pH value leads to the formation of CRT crystals and sodium chloride, which is dissolved in water [12] and eliminated from the system after filtration and washing with deionized water. After filtration and washing with deionized water, the majority of sodium chloride is removed from the solution. However, in some experiments, a small amount of chloride persists in the system with the obtained form of CRT, which is visible in the XRD spectra at 31.78°. The calculated solubility, efficiency expressed as a percentage of CRT crystallized from the solution, and the resulting crystal structures are shown in Table 2.

**Table 2.** Solubility of CRT dihydrochloride in solvent systems with different amounts of water at 25 °C, percentage of CRT crystallized by pH adjustment, and the resulting crystalline form of CRT.

Solvent System	$c_{\text{sat}} \text{ gCRT/g}_{\text{solvent}}$	$\eta, \%$	Crystal Shape
IP–W 1:3	0.227	64.04	-
IP–W 3:2	0.159	80.64	-
IP–W 4:1	0.078	15.53	-
EtOH–W 1:3	0.212	92.63	B + dihydrochloride
EtOH–W 1:1	0.186	94.76	B/C + dihydrochloride
EtOH–W 3:1	0.127	97.00	B/C
AC–W 1:3	0.200	85.15	Mixture of polymorphs
AC–W 1:1	0.146	94.17	B + dihydrochloride
AC–W 3:1	0.076	95.27	A

AC—acetone, EtOH—ethanol, IP—isoopropanol, W—water.

The crystallization in the IP–W system did not result in the formation of crystals but, instead, a muddy precipitate that did not exhibit crystalline properties during the process or after drying. On the other hand, crystallization in the AC–W and EtOH–W systems led to the formation of different forms of CRT, with pure form A being formed in the AC–W 3:1 system and a mixture of forms B and C in the EtOH–W 3:1 system. Even though crystal formation occurred in the AC–W and EtOH–W systems at other volume ratios, these systems were discarded because the X-ray diffractograms contained a characteristic peak of residual dihydrochloride at 31.78 degrees, which decreases API purity. Given that the same results were obtained in repeated experiments, it can be assumed that CRT without residual

dihydrochloride is not generated in systems with a higher proportion of water (>50%). Due to the formation of pure CRT and satisfactory efficiency, the AC–W and EtOH–W systems at a 3:1 volume ratio were chosen for further investigation and the solubility of CRT dihydrochloride in the aforementioned systems was determined at temperatures of 35 and 45 °C. The results are shown in Table 3.

**Table 3.** Solubility of CRT dihydrochloride in AC–W 3:1 and EtOH–W 3:1 solvent systems at 35 and 45 °C, percentage of CRT crystallized by pH adjustment, and the resulting crystalline form of CRT.

Solvent System	T (°C)	$c_{\text{sat}}$ , g <sub>CRT</sub> /g <sub>solvent</sub>	$\eta$ , %	Crystal Shape
AC–W 3:1	35	0.211	76.29	A
AC–W 3:1	45	0.262	76.38	
EtOH–W 3:1	35	0.213	76.95	B/C
EtOH–W 3:1	45	0.237	77.13	

AC—acetone, EtOH—ethanol, W—water.

To investigate the influence of the initial saturation temperature on the size and shape of the produced crystals, crystallization was carried out in solutions saturated at 35 and 45 °C. Similar yields were obtained in both solvent systems, but the values are lower than those for experiments conducted at 25 °C (Table 2). This is most likely due to the fact that the experiments at 25 °C were carried out in glasses with a small volume (50 mL), as opposed to other experiments that were carried out in crystallizers with a larger volume (200 mL), which resulted in higher losses. Micrographs (Figure 1) and PSDs (Figure 2) show that the increase in the saturation temperature leads to the formation of larger crystals obtained from the AC–W 3:1 solvent system. In the EtOH–W 3:1 system, there is no significant variation in crystal size. In both systems, the PSDs are multimodal with a broad or very broad range (Table 4). The method is carried out at high cooling rates and involves the slow introduction of NaOH solution, which leads to a decrease in supersaturation within the solvent mixture and the occurrence of secondary nucleation. It is evident that larger and more regularly shaped crystals of CRT were formed in the AC–W 3:1 system than in the EtOH–W 3:1 system (Figure 1). Changing the solvent has an impact on both the appearance of polymorphism and the crystal growth itself because the growth of crystals in solutions is influenced not only by interactions between the molecules of the dissolved substance but also by interactions between solvent molecules and the surface of the crystal. Faster growth is typically caused by stronger solute–surface contacts than solvent–surface interactions [13]. A further indicator of faster crystal formation is a change in the turbidity of the solution. The turbidity increased almost immediately after the addition of sodium hydroxide to the AC–W 3:1 system, indicating that crystal formation and nucleation occurred more quickly than in the EtOH–W 3:1 system.

**Table 4.** Effect of temperature and solvent system on granulometric properties of CRT crystals obtained from CRT dihydrochloride.

Solvent System	T, °C	$d_{10}$ , $\mu\text{m}$	$d_{50}$ , $\mu\text{m}$	$d_{90}$ , $\mu\text{m}$	S
AC–W 3:1	35	5.583	26.652	92.440	16.557
	45	14.705	49.116	101.596	6.909
EtOH–W 3:1	35	1.249	5.841	13.966	11.182
	45	1.796	6.440	17.865	9.947

AC—acetone, EtOH—ethanol, W—water.

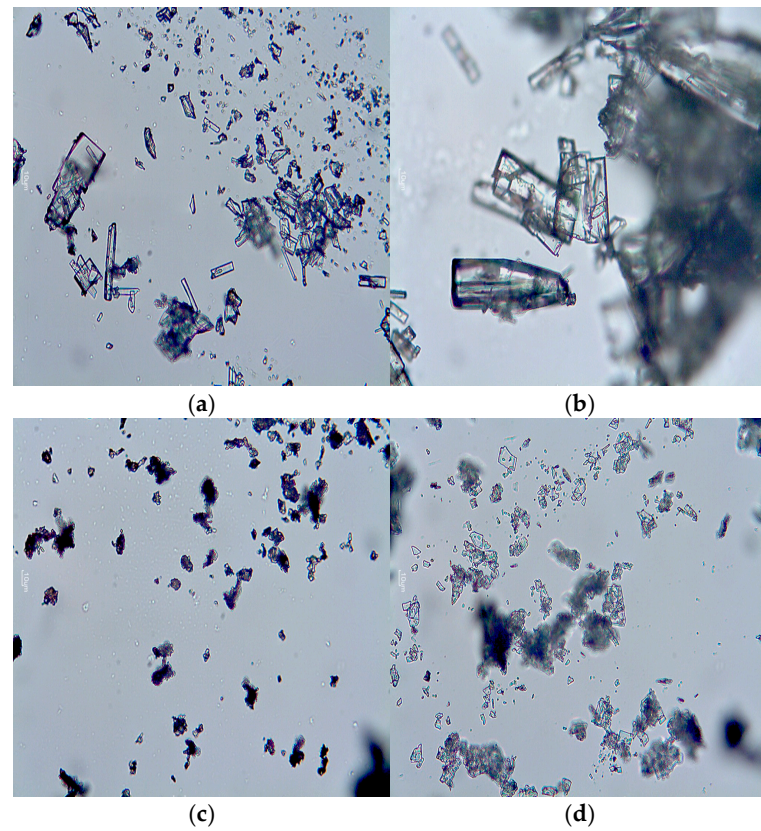


**Figure 1.** Micrographs of CRT crystals obtained from the AC–W 3:1 solvent system at (a) 35, (b) 45, and from the EtOH–W 3:1 solvent system at (c) 35, (d) 45 °C (400× magnification).

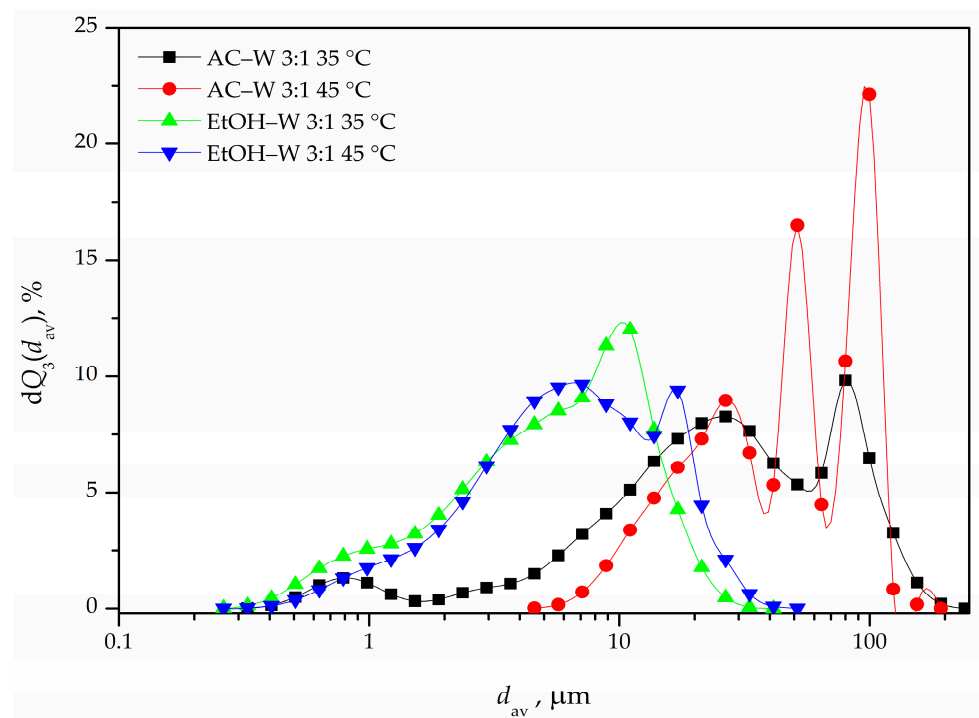


**Figure 2.** PSDs of CRT crystals obtained from the AC–W 3:1 and EtOH–W 3:1 solvent systems at 35 and 45 °C.

The obtained X-ray diffractograms show that the change in the initial crystallization temperature did not affect the crystal structure of CRT as characteristic peaks of form A are present at 7.2, 7.9, 13.4, 14.4, 18.5, 19.0 degrees (Figure 3) and of forms B and C at 9.6, 14.5, 15.1, 19.0, 28.3, and 29.0 and 5.5, 9.4, 12.5, 16.5, and 25.1, respectively (Figure 4) [9,14]. Furthermore, the AC–W 3:1 solvent system was the only one that produced a pure form of CRT. Therefore, form A was chosen for further recrystallization of CRT.

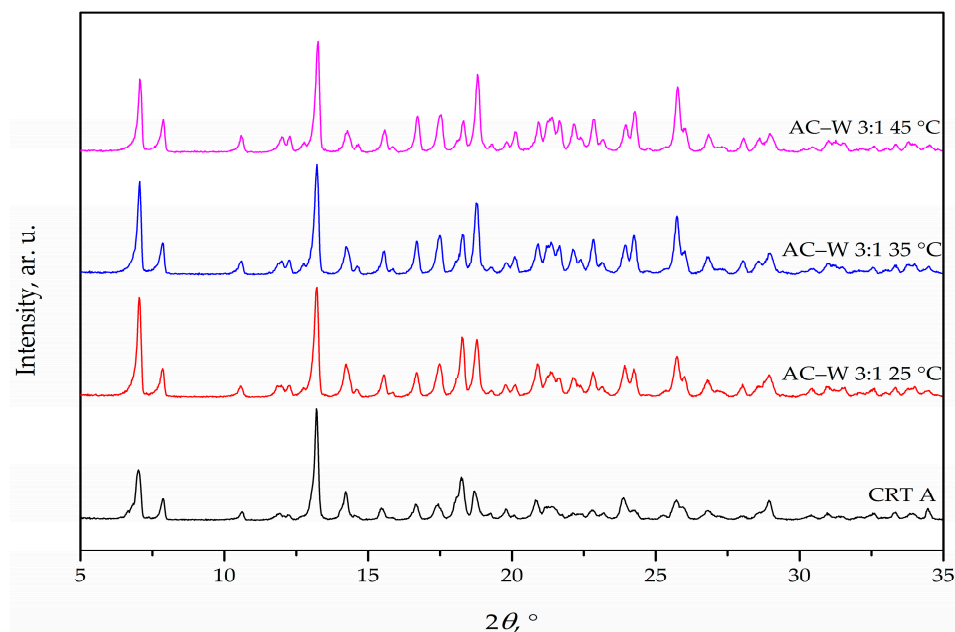


**Figure 3.** XRD spectra of CRT form A obtained in the AC–W 3:1 solvent system at 25, 35, and 45 °C.

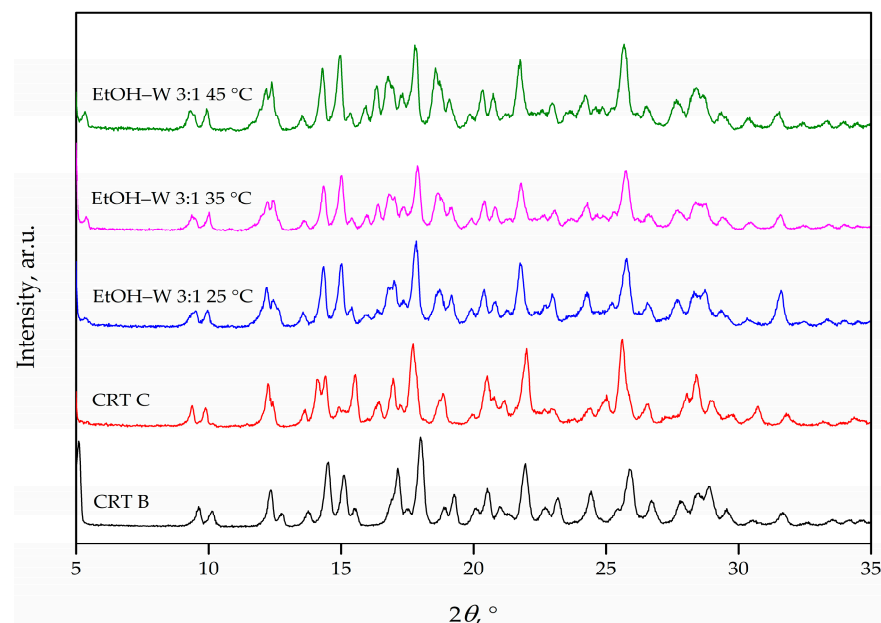


**Figure 4.** XRD spectra of CRT forms B and C obtained in the EtOH–W 3:1 solvent system at 25, 35, and 45 °C.

### 3.2. Solubility and Recrystallization of CRT Form A

The presence of irregular and plate-like crystals can lead to difficulties in downstream processing and product quality issues. Additionally, the broad distribution of particle

size can affect the performance and stability of the final product. Therefore, it is crucial to carefully control the crystallization conditions to ensure the formation of uniform and well-defined crystals with a narrow PSD. In order to improve the obtained granulometric properties of CRT crystals, the recrystallization of CRT form A was preceded by the selection of a suitable solvent following the solvent selection guide. The solubility of CRT form A was determined at 35 °C in acetone, ethanol, isopropanol, methanol, THF, and water, the results of which are shown in Table 5.

**Table 5.** Solubility of CRT form A in water and different organic solvents at 35 °C.

Solvent	$c_{\text{sat}}, \text{g}_{\text{CRT}}/\text{g}_{\text{solvent}}$
THF	0.163
AC	0.026
MetOH	0.046
IP	0.044
EtOH	0.028
W	<0.001

AC—acetone, EtOH—ethanol, IP—isoopropanol, MetOH—methanol, THF—tetrahydrofuran, W—water.

Since CRT form A exhibited the highest solubility in THF, its solubility was determined in the range of 5–55 °C in order to construct a solubility curve (Figure 5) and assess the thermodynamic characteristics of the dissolution process. Using the experimentally obtained data, mole fraction solubility of CRT in THF at different temperatures was calculated using Equation (1) and then correlated with the modified Apelblat model:

$$\ln x = A + \frac{B}{T} + C \ln T \quad (2)$$

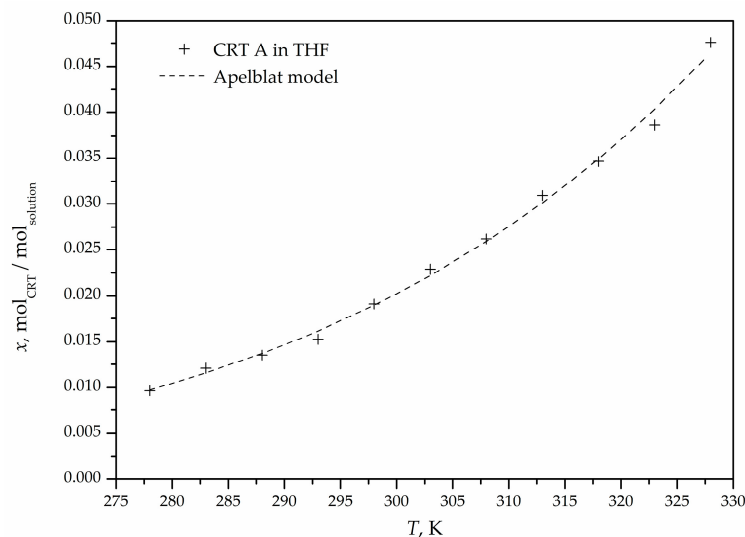


**Figure 5.** The solubility curve of CRT in THF and the correlation with the modified Apelblat model.

The modified Apelblat model (Equation (2)) describes the relationship between the mole fraction solubility of a substance and temperature [15,16]. The regression parameters  $A$ ,  $B$ , and  $C$  were estimated using the Excel add-in Solver.

The relative deviation (RD) and relative average deviation (RAD) were calculated to determine the suitability of the modified Apelblat model for describing this particular process. RD and RAD values were calculated by the following equations:

$$\text{RD} = \frac{x_{i, \text{exp}} - x_{i, \text{cal}}}{x_{i, \text{exp}}} \quad (3)$$

$$\text{RAD} = \frac{1}{N} \sqrt{\sum_{i=1}^N \left( \frac{x_{\text{cal}} - x_{\text{exp}}}{x_{\text{exp}}} \right)^2} \quad (4)$$

where  $x_{\text{exp}}$  and  $x_{\text{cal}}$  represent the experimental and calculated mole fraction solubility values, and  $N$  represents the number of measurements in the experiment. The experimental and calculated mole fraction solubilities ( $x_{\text{exp}}$  and  $x_{\text{cal}}$ ), RD and RAD values, as well as the regression parameters  $A$ ,  $B$ , and  $C$ , are shown in Table 6. The resulting RD and RAD values, along with the graphical correlation of the experimental and calculated solubility data (Figure 5), demonstrate a high level of agreement. Consequently, it can be concluded that the modified Apelblat model is well suited for describing the dissolution behavior of CRT form A in THF.

**Table 6.** Experimental and calculated mole fraction solubility of CRT form A in THF at different temperatures, RD and RMSD values, and regression parameters of the modified Apelblat model.

THF							
Apelblat Model							
$T, \text{K}$	$x_{\text{exp}}$	$x_{\text{cal}}$	RD	$A$	$B$	$C$	RAD
278	0.00966	0.00974	$-8.00 \times 10^{-3}$				
283	0.01209	0.01157	$4.27 \times 10^{-2}$				
288	0.01352	0.01369	$-1.32 \times 10^{-2}$				
293	0.01527	0.01746	$-1.44 \times 10^{-1}$				
298	0.01910	0.01990	$-4.21 \times 10^{-2}$				
303	0.02288	0.02265	$9.93 \times 10^{-3}$	-36.86	-941.31	6.33	$8.91 \times 10^{-3}$
308	0.02617	0.02573	$1.66 \times 10^{-2}$				
313	0.03092	0.02918	$5.63 \times 10^{-2}$				
318	0.03463	0.03304	$4.59 \times 10^{-2}$				
323	0.03863	0.03734	$3.32 \times 10^{-2}$				
328	0.03945	0.04214	$-6.82 \times 10^{-2}$				

The results and the regression parameters of the modified Apelblat model (Table 6) were used for the thermodynamic analysis of the dissolution process. The thermodynamic properties of the dissolution of CRT form A in THF were described using the Gibbs free energy ( $\Delta G_{\text{sol}}$ ), standard molar dissolution enthalpy ( $\Delta H_{\text{sol}}$ ), and standard dissolution entropy ( $\Delta S_{\text{sol}}$ ), which were calculated using Equations (5)–(7):

$$\Delta H_{\text{sol}} = RT \left( C - \frac{B}{T} \right) \quad (5)$$

$$\Delta G_{\text{sol}} = -RT \left( A + \frac{B}{T} + C \ln T \right) \quad (6)$$

$$\Delta S_{\text{sol}} = R(A + C + C \ln T) \quad (7)$$

where  $R$  is the molar gas constant,  $A$ ,  $B$ , and  $C$  are regression parameters of the modified Apelblat model, and  $T$  is the mean arithmetic temperature for the observed temperature range. The relative contribution of enthalpy ( $\% \zeta_H$ ) and entropy ( $\% \zeta_{TS}$ ) was calculated by following equations:

$$\% \zeta_H = \frac{|\Delta H_{\text{sol}}|}{|\Delta H_{\text{sol}}| + |T \Delta S_{\text{sol}}|} \times 100 \quad (8)$$

$$\% \zeta_{TS} = \frac{|T \Delta S_{\text{sol}}|}{|\Delta H_{\text{sol}}| + |T \Delta S_{\text{sol}}|} \times 100 \quad (9)$$

The results are shown in Table 7.

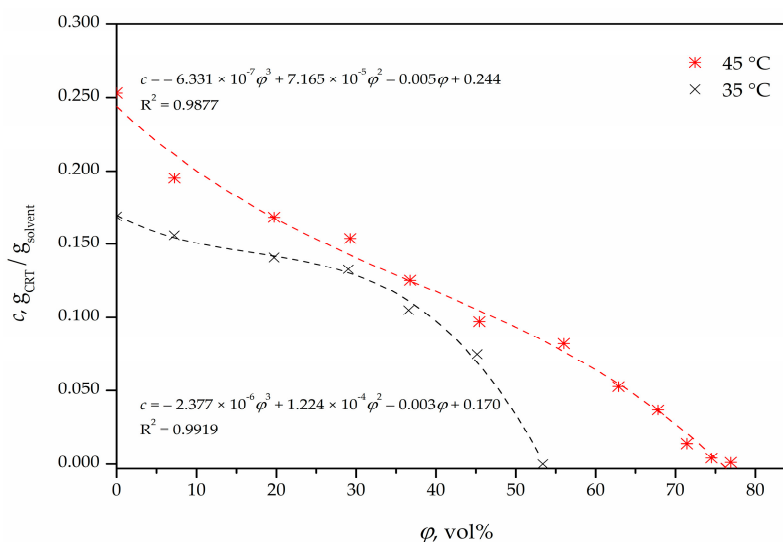
**Table 7.** Thermodynamic properties for the dissolution of CRT form A in THF.

Solvent	T, K	$\Delta H_{\text{sol}}$ , kJ/mol	$\Delta S_{\text{sol}}$ , kJ/(mol·K)	$\Delta G_{\text{sol}}$ , kJ/mol	% $\zeta_{\text{H}}$	% $\zeta_{\text{TS}}$
THF	303.00	23.77	0.05	9.59	62.64	37.36

Standard uncertainties,  $u$ , are  $u(\Delta H_{\text{sol}}) = 0.24$  kJ/mol,  $u(\Delta S_{\text{sol}}) = 0.0009$  kJ/(mol·K) and  $u(\Delta G_{\text{sol}}) = 0.03$  kJ/mol.

The values of  $\Delta H_{\text{sol}}$  and  $\Delta G_{\text{sol}}$  are both positive for the dissolution of CRT form A in THF, which indicates that the process is endothermic, while the positive value of  $\Delta S_{\text{sol}}$  indicates that the process is driven by entropy. The value of % $\zeta_{\text{H}}$  (62.64%) is higher than the value of % $\zeta_{\text{TS}}$  (37.36%), which indicates that the enthalpy is the main contributor to changes in the standard Gibbs energy during the dissolution of CRT form A in THF [17–19].

After determining the solubility in THF, recrystallization was performed by antisolvent crystallization to further purify the API. Antisolvent crystallization was chosen as the crystallization method because it is typically used to crystallize poorly water-soluble drugs in order to alter the physical properties of the drug, such as crystalline structure or PSD [20]. As CRT form A dissolves best in THF (Table 5), which is classified as a usable solvent in the solvent selection guide, it was chosen as the solvent for the recrystallization of CRT. Water was chosen as the antisolvent, because CRT form A showed extremely low solubility in it, and because water mixes well with the selected polar solvent (THF). In both experiments, the antisolvent was added at the same rate of 3 mL/min via a syringe pump in order to determine the influence of the initial saturation temperature on the kinetics of antisolvent crystallization of CRT. The experimental data of concentration in relation to the proportion of water during the recrystallization process of CRT were fitted using a third-degree polynomial. The resulting curves with associated equations and R-Squared values are shown in Figure 6.

**Figure 6.** Dependence of CRT concentration with the volume fraction of added water.

When the precipitation is carried out at higher temperatures, the proportion of water needed to completely crystallize the dissolved CRT is larger due to higher saturation. Over 50 vol% of water was added to the THF solution saturated at 35 °C, but at 45 °C, the amount was roughly 80 vol% (Figure 6). Since the rate of water addition is the same for both tested temperatures, the process at a higher temperature lasts longer, which impacts the granulometric characteristics of the produced crystals (Figures 7 and 8). In both experiments, larger, more compact crystals were produced during recrystallization, and the PSDs were narrower (Table 8). Furthermore, it is obvious that the proportion of small particles is higher for the process conducted at a lower temperature. Low temperatures decrease drug solubility in

solvent–antisolvent mixtures, leading to higher supersaturation conditions. This decreases diffusion and growth kinetics at the crystal boundary layer interface, resulting in formation of smaller drug particles [20]. The obtained X-ray diffractograms (Figure 9) show that the recrystallization from THF did not affect the crystal structure of CRT as characteristic peaks of CRT form A are present at 7.2, 7.9, 13.4, 14.4, 18.5, and 19.0 degrees [9,14].

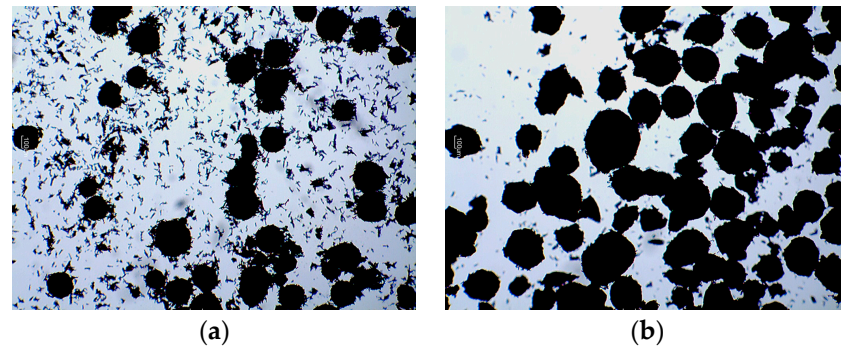


**Figure 7.** Micrographs of CRT form A after recrystallization from THF solutions saturated at (a) 35 and (b) 45 °C (40× magnification).

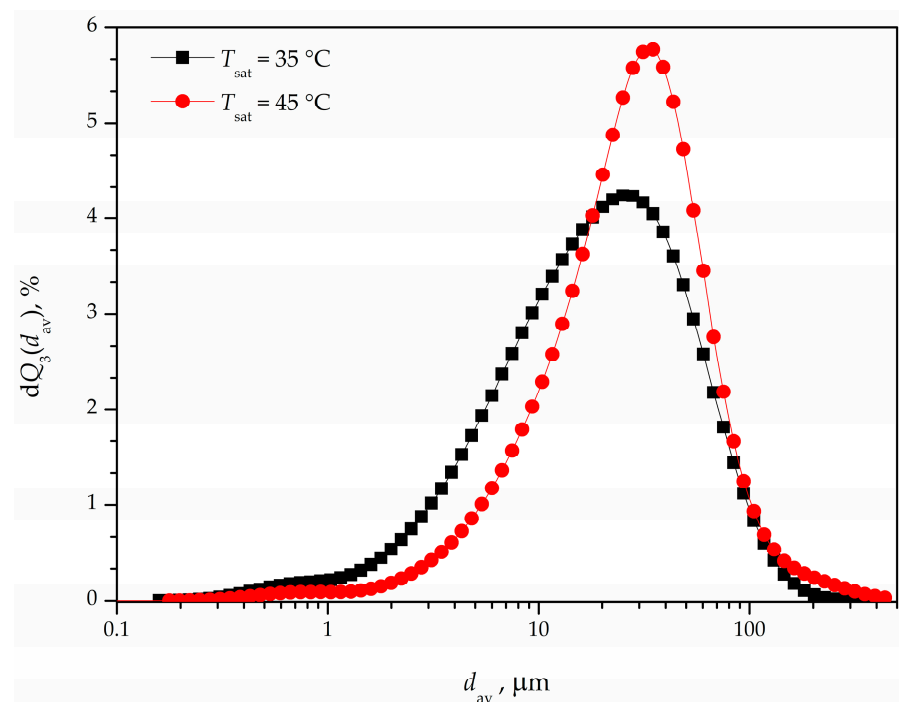


**Figure 8.** PSDs of CRT crystals obtained by recrystallization from THF solutions saturated at 35 and 45 °C.

**Table 8.** Effect of temperature and solvent system on granulometric properties of CRT crystals.

Solvent	$T_{sat}$ , °C	$d_{10}$ , $\mu\text{m}$	$d_{50}$ , $\mu\text{m}$	$d_{90}$ , $\mu\text{m}$	S
THF	35	4.180	19.209	61.985	14.830
	45	7.910	26.742	70.057	8.857

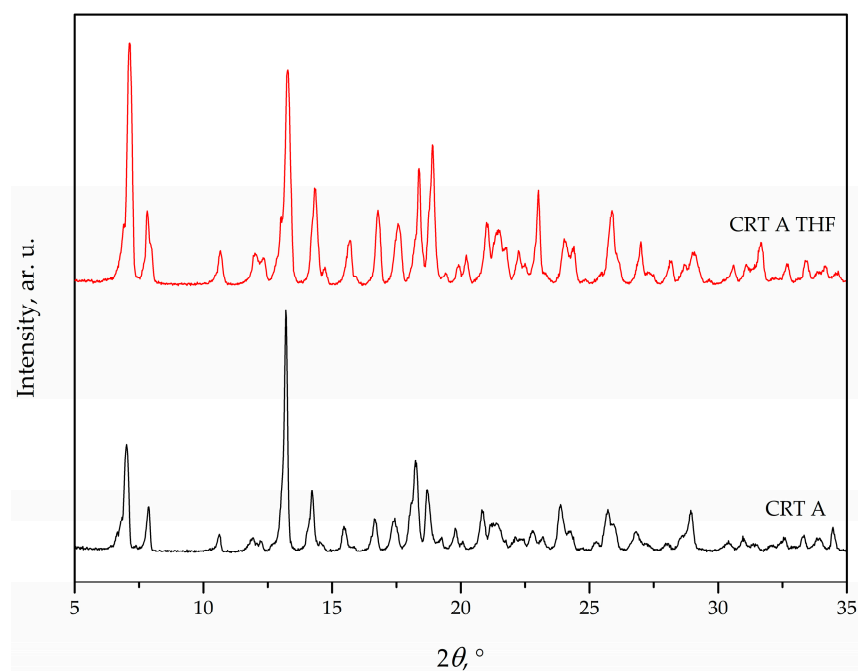


**Figure 9.** XRD spectra of CRT form A before and after recrystallization from THF by antisolvent addition.

### 3.3. Kinetics of Drying

After crystallization, it can be very challenging to obtain a dry API. The filtration and drying operations may be hindered by variations in crystal size and shape. Crystals that do not grow equally in all directions result in needle-like or plate-like crystal shapes that then slow down filtration and drying processes. Since the crystals obtained after recrystallization in THF are compact and have a uniform PSD, it was expected that the filtration and drying processes would be easily carried out. Both the time of filtration and the initial cake moisture were significantly lower for crystals produced at 45 °C than for crystals produced at 35 °C. (Table 9). The crystals produced at a higher saturation temperature were larger and had a narrower PSD, which affected the initial moisture content of the obtained filter cakes and, consequently, their drying. The normalized drying curves (Figure 10) show that larger crystals dry much faster and at a lower maximum rate than smaller crystals. It is expected that the material with a narrower PSD and larger particles will dry faster, since moisture moves faster through the material's larger pores. However, because of the lower initial humidity, the driving force is decreased, as is the maximum drying rate [21].

**Table 9.** Drying time, initial and critical moisture content, and maximum drying rate of CRT crystals obtained by recrystallization from THF solutions saturated at 35 and 45 °C.

$T_{\text{sat}}, \text{ }^\circ\text{C}$	$t, \text{ s}$	$X_0, \text{ g/g}$	$X_{\text{cr}}, \text{ g/g}$	$dX/dt, \text{ g}_w/(\text{g}_{\text{dm}} \cdot \text{s})$
35	1560	0.9185	0.4045	$8.20 \times 10^{-4}$
45	840	0.3723	0.1282	$6.66 \times 10^{-4}$

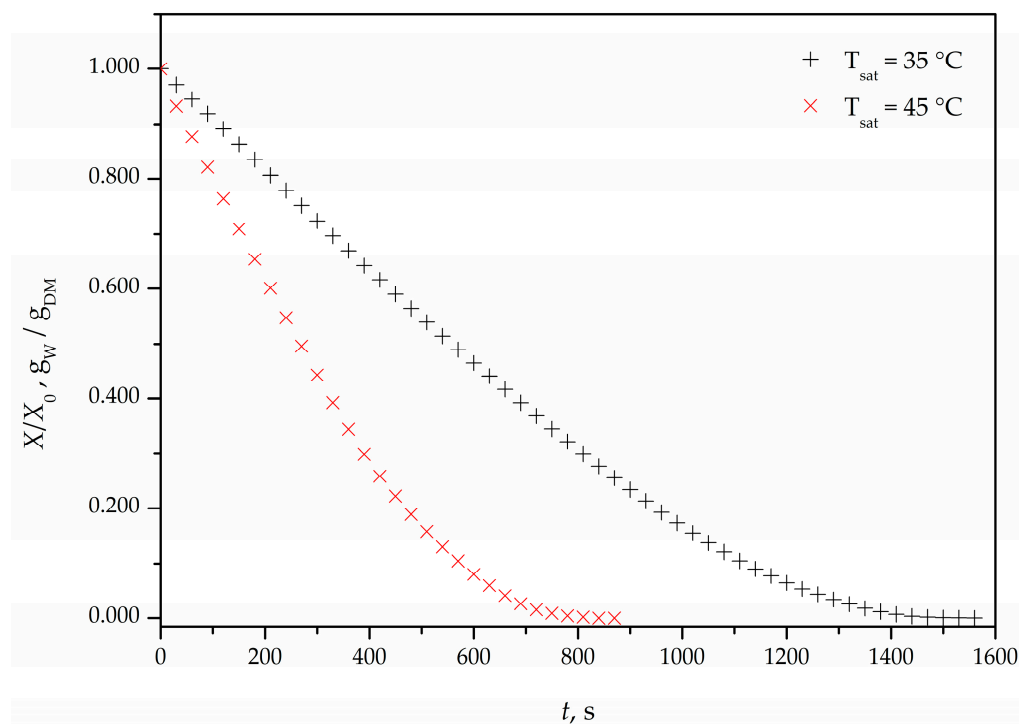


**Figure 10.** The influence of saturation temperature on drying kinetics of CRT at 60 °C.

#### 4. Conclusions

By using pH adjustment combined with cooling crystallization, multiple polymorphs of CRT can be produced from CRT dihydrochloride in various solvent systems. Crystals were isolated at pH = 11, while the appearance of polymorphs was dependent on the solvent used. Only the AC–W 3:1 system generated pure form A, and increasing the saturation temperature resulted in the formation of larger crystals. The PSD of the developed CRT crystals was broad and multimodal. The crystals' solubility in various solvents was investigated in an effort to enhance their granulometric properties. CRT is most soluble in THF, so this solvent was chosen for recrystallization, whereas water was used as an antisolvent. Furthermore, the effect of saturation temperature on the granulometric characteristics and internal structure of the crystals was investigated. Larger crystals with narrower PSD were produced when crystallization was carried out at higher saturation temperatures, which benefited filtration and drying processes. The obtained X-ray diffractograms showed that the change in the initial crystallization temperature did not affect the crystal structure of CRT.

**Author Contributions:** Conceptualization, I.Z. and J.P.K.; Data curation, I.Z. and J.P.K.; Investigation, I.Z. and J.P.K.; Methodology, I.Z. and J.P.K.; Supervision, J.P.K.; Writing—original draft, I.Z. and J.P.K.; Writing—review and editing, I.Z. and J.P.K. All authors have read and agreed to the published version of the manuscript.

**Funding:** This research is funded by European Structural and Investment Funds, grant number KK.01.1.1.07.0017 (CrystAPC—Crystallization Advanced Process Control).

**Data Availability Statement:** Data available on request.

**Conflicts of Interest:** The authors declare no conflict of interest.

## Abbreviations

AC	acetone
ALK	anaplastic lymphoma kinase
API	active pharmaceutical ingredient
BCS	Biopharmaceutics Classification System
CRT	ceritinib
EtOH	ethanol
IP	isopropanol
MetOH	methanol
PSD	particle size distribution
RAD	relative average deviation
RD	relative deviation
THF	tetrahydrofuran
W	water
XRD	X-ray powder diffraction

## Symbols

$A, B, C$	[-]	regression parameters of the modified Apelblat model
$c$	[g <sub>CRT</sub> /g <sub>solvent</sub> ]	concentration
$d$	[ $\mu\text{m}$ ]	particle size
$dQ(d)$	[%]	function of volume fraction
$M_{\text{CRT}}$	[g/mol]	molar mass of ceritinib
$m_{\text{CRT}}$	[g]	mass of ceritinib
$M_{\text{THF}}$	[g/mol]	molar mass of tetrahydrofuran
$m_{\text{THF}}$	[g]	mass of tetrahydrofuran
$S$	[-]	distribution width
$T$	[K]	temperature
$t$	[s]	time
$u$	[kJ/mol; kJ/(mol·K)]	standard uncertainty
$x$	[mol <sub>CRT</sub> /mol <sub>solution</sub> ]	mole fraction solubility
$X$	[g <sub>W</sub> /g <sub>DM</sub> ]	material moisture content
$\Delta G$	[kJ/mol]	Gibbs free energy
$\Delta H$	[kJ/mol]	molar dissolution enthalpy
$\Delta S$	[kJ/(mol K)]	molar dissolution entropy

## Greek letters

$\% \zeta$	[%]	relative contribution
$\eta$	[%]	efficiency
$\varphi$	[%]	volume ratio
$\lambda$	[ $\text{\AA}$ ]	wavelength
$\theta$	[ $^{\circ}$ ]	angle of diffraction

## Sub- and superscripts

0	initial
av	average
cal	calculated
cr	critical
exp	experimental
H	enthalpy
sat	saturation
sol	solubility
TS	entropy

## References

- Chen, J.; Sarma, B.; Evans, J.M.B.; Myerson, A.S. Pharmaceutical Crystallization. *Cryst. Growth Des.* **2011**, *11*, 887–895. [[CrossRef](#)]
- Hrkovac, M.; Kardum, J.P.; Ukrainczyk, N. Influence of NaCl on Granulometric Characteristics and Polymorphism in Batch-Cooling Crystallization of Glycine. *Chem. Eng. Technol.* **2015**, *38*, 139–146. [[CrossRef](#)]
- Taylor, L.S.; Braun, D.E.; Steed, J.W. Crystals and Crystallization in Drug Delivery Design. *Mol. Pharm.* **2021**, *18*, 751–753. [[CrossRef](#)] [[PubMed](#)]

4. Ter Horst, J.H.; Geertman, R.M.; Van Rosmalen, G.M. The Effect of Solvent on Crystal Morphology. *J. Cryst. Growth* **2001**, *230*, 277–284. [[CrossRef](#)]
5. Rosbottom, I.; Ma, C.Y.; Turner, T.D.; O’Connell, R.A.; Loughrey, J.; Sadiq, G.; Davey, R.J.; Roberts, K.J. Influence of Solvent Composition on the Crystal Morphology and Structure of *p*-Aminobenzoic Acid Crystallized from Mixed Ethanol and Nitromethane Solutions. *Cryst. Growth Des.* **2017**, *17*, 4151–4161. [[CrossRef](#)]
6. Croker, D.M.; Kelly, D.M.; Horgan, D.E.; Hodnett, B.K.; Lawrence, S.E.; Moynihan, H.A.; Rasmuson, Å.C. Demonstrating the Influence of Solvent Choice and Crystallization Conditions on Phenacetin Crystal Habit and Particle Size Distribution. *Org. Process Res. Dev.* **2015**, *19*, 1826–1836. [[CrossRef](#)]
7. Lu, J.; Rohani, S. Polymorphism and Crystallization of Active Pharmaceutical Ingredients (APIs). *CMC* **2009**, *16*, 884–905. [[CrossRef](#)]
8. Chennuru, R.; Koya, R.T.; Kommavarapu, P.; Narasayya, S.V.; Muthudoss, P.; Vishweshwar, P.; Babu, R.R.C.; Mahapatra, S. In Situ Metastable Form: A Route for the Generation of Hydrate and Anhydrous Forms of Ceritinib. *Cryst. Growth Des.* **2017**, *17*, 6341–6352. [[CrossRef](#)]
9. Grebenar, I.; Ratkaj, M.; Mundorfer, T.; Nežić, I. Solid State Forms of Ceritinib and Salts Thereof. WO2016081538A1, 26 May 2016. Available online: <https://patents.google.com/patent/WO2016081538A1/en> (accessed on 8 June 2023).
10. Nishio, M.; Murakami, H.; Horiike, A.; Takahashi, T.; Hirai, F.; Suenaga, N.; Tajima, T.; Tokushige, K.; Ishii, M.; Boral, A.; et al. Phase I Study of Ceritinib (LDK378) in Japanese Patients with Advanced, Anaplastic Lymphoma Kinase-Rearranged Non-Small-Cell Lung Cancer or Other Tumors. *J. Thorac. Oncol.* **2015**, *10*, 1058–1066. [[CrossRef](#)] [[PubMed](#)]
11. Takagi, T.; Ramachandran, C.; Bermejo, M.; Yamashita, S.; Yu, L.X.; Amidon, G.L. A Provisional Biopharmaceutical Classification of the Top 200 Oral Drug Products in the United States, Great Britain, Spain, and Japan. *Mol. Pharm.* **2006**, *3*, 631–643. [[CrossRef](#)] [[PubMed](#)]
12. Langer, H.; Offermann, H. On the Solubility of Sodium Chloride in Water. *J. Cryst. Growth* **1982**, *60*, 389–392. [[CrossRef](#)]
13. Zhang, C.; Ji, C.; Li, H.; Zhou, Y.; Xu, J.; Xu, R.; Li, J.; Luo, Y. Occupancy Model for Predicting the Crystal Morphologies Influenced by Solvents and Temperature, and Its Application to Nitroamine Explosives. *Cryst. Growth Des.* **2013**, *13*, 282–290. [[CrossRef](#)]
14. Feng, L.; Gong, B.; Karpinski, P.H.; Waykole, L.M. Crystalline Forms of 5-Chloro-N2-(2-Isopropoxy-5-Methyl-4-Piperidin-4-Yl-Phenyl)-N4-[2-(Propane-2-Sulfonyl)-Phenyl]-Pyrimidine-2,4-Diamine. US20130274279A1, 17 October 2013. Available online: <https://patents.google.com/patent/US20130274279A1/en> (accessed on 7 September 2023).
15. Ha, E.-S.; Lee, Y.-R.; Kim, M.-S. Solubility of Dronedarone Hydrochloride in Six Pure Solvents at the Range of 298.15 to 323.15 K. *J. Mol. Liq.* **2016**, *216*, 360–363. [[CrossRef](#)]
16. Ren, J.; Chen, D.; Yu, Y.; Li, H. Solubility of Dicarbohydrazide Bis[3-(5-Nitroimino-1,2,4-Triazole)] in Common Pure Solvents and Binary Solvents at Different Temperatures. *R. Soc. Open Sci.* **2019**, *6*, 190728. [[CrossRef](#)]
17. Cheng, Y.; Wang, D.; Zhang, Z.; Wang, Z. Solubility and Solution Thermodynamics of Rhein in Eight Pure Solvents from (288.15 to 313.15) K. *RSC Adv.* **2015**, *5*, 80548–80552. [[CrossRef](#)]
18. Liang, M.; Hu, Y.; Liu, X.; Guan, J.; Yang, W.; Liu, Y. Solubility of Maleic Anhydride in Methanol+(Acetone, Ethyl Acetate) from 278.15 to 323.15 K. *J. Mol. Liq.* **2014**, *197*, 35–39. [[CrossRef](#)]
19. Li, R.; Zhang, B.; Hou, N.; Li, C.; Xie, J.; He, J.; Chen, X.; Xu, Q.; Zhao, J.; Han, D. The Solubility Profile and Apparent Thermodynamic Analysis of Doxofylline in Pure and Mixed Solvents. *J. Chem. Thermodyn.* **2020**, *148*, 106126. [[CrossRef](#)]
20. Lonare, A.A.; Patel, S.R. Antisolvent Crystallization of Poorly Water Soluble Drugs. *IJCEA* **2013**, *4*, 337–341. [[CrossRef](#)]
21. Prlic Kardum, J.; Sander, A. Drying of Pentaerythritol Obtained from Batch Crystallization. *Chem. Eng. Technol.* **2010**, *33*, 812–820. [[CrossRef](#)]

**Disclaimer/Publisher’s Note:** The statements, opinions and data contained in all publications are solely those of the individual author(s) and contributor(s) and not of MDPI and/or the editor(s). MDPI and/or the editor(s) disclaim responsibility for any injury to people or property resulting from any ideas, methods, instructions or products referred to in the content.